Molecular dynamics simulations of shock waves using the absorbing boundary condition: A case study of methane

Alexey V. Bolesta,* Lianqing Zheng,† and Donald L. Thompson‡
Department of Chemistry, University of Missouri-Columbia, Columbia, Missouri 65211, USA

Thomas D. Sewell§
Theoretical Division, Los Alamos National Laboratory, Los Alamos, New Mexico 87545, USA
(Received 5 April 2007; revised manuscript received 19 September 2007; published 14 December 2007)

We report a method that enables long-time molecular dynamics (MD) simulations of shock wave loading. The goal is to mitigate the severe interference effects that arise at interfaces or free boundaries when using standard nonequilibrium MD shock wave approaches. The essence of the method is to capture between two fixed pistons the material state at the precise instant in time when the shock front, initiated by a piston with velocity u_p at one end of the target sample, traverses the contiguous boundary between the target and a second, stationary piston located at the opposite end of the sample, at which point the second piston is also assigned velocity u_p and the simulation is continued. Thus, the target material is captured in the energy-volume Hugoniot state resulting from the initial shock wave, and can be propagated forward in time to monitor any subsequent chemistry, plastic deformation, or other time-dependent phenomena compatible with the spatial scale of the simulation. For demonstration purposes, we apply the method to shock-induced chemistry in methane based on the adaptive intermolecular reactive empirical bond order force field [S. J. Stuart *et al.*, J. Chem. Phys. **112**, 6472 (2000)].

DOI: 10.1103/PhysRevB.76.224108 PACS number(s): 62.50.+p, 82.20.Wt, 82.40.Fp

I. INTRODUCTION

Dynamic material response to shock wave loading has been studied for decades for both practical and fundamental reasons.[1] Molecular dynamics (MD) is the most widely used method for theoretical studies of physical and chemical processes in condensed materials on submicron scales. Since the 1970s, nonequilibrium molecular dynamics (NEMD) has been applied to studies of shock-induced phenomena such as defect generation,[2] phase transitions,[3] and chemistry.[4,5] Although current computer capabilities allow shock wave simulations for systems containing even billions of atoms interacting via comparatively simple potentials (for instance, the embedded-atom model),[6] it is computationally expensive to use NEMD to study shock waves in complicated, polyatomic molecular crystals characterized by many-body interactions and electrostatic contributions to the potential energy.[7] This is particularly true since many of the phenomena of interest occur on time scales significantly larger than those required for the passage of a shock wave through a typical MD simulation cell.

Various equilibrium MD methods, sometimes called Hugoniostat methods, have been developed in the past decade to reproduce the final states of shocked materials by way of extended equations of motion that act on the system to drive it toward a prescribed Hugoniot state.[8–12] (The Hugoniot is the locus of states accessible by shock wave loading.) This allows long-time sampling of shock states without the need to simulate a system that is large enough to sustain the compressed state for a long enough time to arrive at those states. In cases where the shock wave dynamics is of interest, however, the Hugoniostat methods are of limited use. Zhakhovskii *et al.*[13] developed a "moving window" method that allows the study of the detailed dynamics in the vicinity of a shock front by systematically adding new material to the unshocked end of the simulation cell and removing shocked material from the other end so that the simulation size remains constant and the simulation frame remains centered on the shock front. However, even this method becomes difficult to apply to simulations with nonprompt chemistry or mechanical deformation, since adding and removing material from the simulation will certainly introduce artifacts for practically accessible simulation domains. Most recently, Zhao *et al.*[14] developed a NEMD method to study shock-induced alloying reactions in Ni/Al nanolaminates. In their method, shock waves are first generated by colliding two identical slabs with equal but opposite center-of-mass velocities. The periodic boundaries along the shock direction shrink consistently with the mass velocity. Once the shock waves reach the periodic boundaries, however, the cell parameters are fixed, and the simulation is continued in the usual three-dimensional periodic, constant energy–constant volume (*NVE*) ensemble to allow the alloying reactions to approach equilibrium.

Here, we report a NEMD method that allows the dynamics behind a shock wave to evolve with minimal interference from the free surface of the simulation cell. We demonstrate the method in a study of shock-induced chemistry in condensed-phase methane based on the adaptive intermolecular reactive empirical bond order (AIREBO) force field.[15]

II. COMPUTATIONAL DETAILS

A. Absorbing boundary condition

A schematic diagram of how the absorbing boundary condition is applied in a simulation of a shock wave is presented

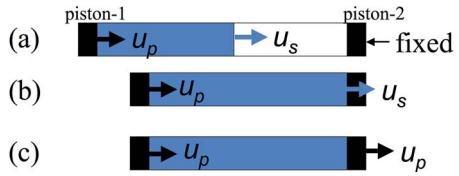

FIG. 1. (Color online) Schematic illustration of how the shock absorbing boundary condition is applied. (a) A shock wave is generated in the sample by driving a rigid piston into it with constant velocity u_p; a second piston is contiguous to and equilibrated with the material on the opposite end of the simulation cell. (b) The shock wave reaches the second piston. (c) The second piston begins to move with the same fixed velocity as the first.

in Fig. 1.[16] By moving a rigid piston (piston-1) at constant velocity u_p, a shock wave is generated that moves with velocity u_s through the target material [see Fig. 1(a)]. On the opposite end of the simulation cell is a second rigid piston (piston-2), contiguous with the target and assigned zero velocity. When the shock wave reaches piston-2 [Fig. 1(b)], it is instantaneously assigned the same constant velocity as piston-1 (u_p) [see Fig. 1(c)]. From that point onward, the simulation is microcanonical and maintains the initial Hugoniot state associated with the passage of the shock front. Chemical reactions or other dynamical processes can be followed until they reach equilibrium. These processes can result in significant changes in temperature, pressure, and composition in the confined region.

A critical issue is exactly when and how to apply the velocity u_p to the second piston. Although various criteria can be imagined, the initial transfer of internal energy is a reasonable one for defining the instant of shock wave passage across a given dividing surface in configuration space since shock wave propagation is essentially energy transfer from the moving piston to lattice degrees of freedom in the target material. We show in Fig. 2 how we use the internal energy to determine the time at which the second piston begins to move. In this case, the piston velocity u_p=3.0 km/s is below the threshold for shock-induced chemistry in methane. The simulation cell is arbitrarily divided into 80 bins, each one unit cell wide; these bins deform affinely as the shock wave compresses the sample. Figure 2(a) contains the internal energy profile in the material along the shock direction at t=5.45 ps, which is just before the internal energy of the bin immediately adjacent to piston-2 begins to rise rapidly [denoted as bin 80, corresponding to zero displacement along the abscissa in Fig. 2(a); the internal energy of this bin is denoted as ε_{80} in Fig. 2(b)]. The internal energy profile of the shocked material in Fig. 2(a) is fitted to a straight line, which is extrapolated to predict the internal energy ε_{80} at the moment when the shock front just reaches its outer edge (that is, the contiguous boundary with the second piston). Monitoring the internal energy ε_{80} as the trajectory continues, we find that the extrapolated value is achieved at t =5.57 ps [see Fig. 2(b)]; the dashed horizontal line in Fig. 2(b) shows the extrapolated value for the internal energy corresponding to the moment when the shock wave reaches piston-2. It is at this time that the second piston begins to move with the same fixed velocity u_p as the first one.

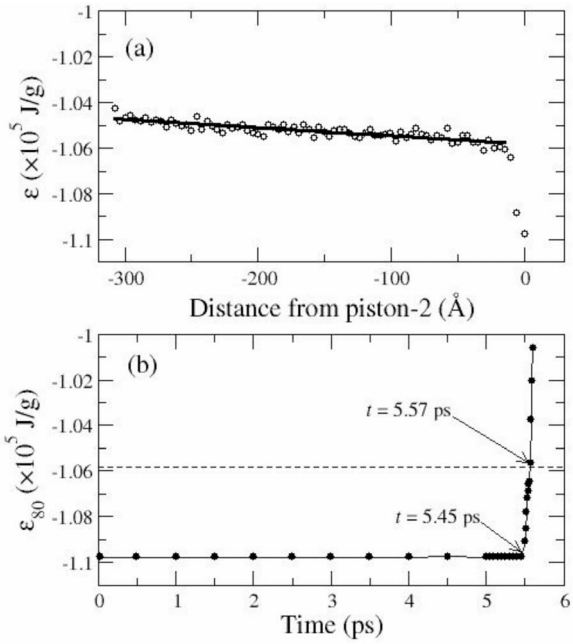

FIG. 2. Summary of details for determining when the second piston begins to move. (a) Internal energy profile along the shock direction; (b) time evolution of internal energy in the material subvolume (bin) closest to the second piston [zero displacement along the abscissa in (a) corresponds to internal energy ε_{80} in (b)]. The time snapshot in (a) is for t=5.45 ps; the line is the linear fit for the shocked material. The dashed horizontal line in (b) shows the extrapolated value for the internal energy, corresponding to the moment when the shock wave reaches piston-2. When the internal energy ε_{80} reaches this value (t=5.57 ps), the second piston is assigned a constant velocity u_p.

There is a significant disparity in the time scales for shock wave traversal of the sample in most NEMD simulations and subsequent establishment of chemical or thermo-mechanical equilibrium. In the simplest sense, the maximum time accessible to the former is the shock transit time across the sample, $t_{max}=l_{sample}/u_s$. However, this only applies to material in the immediate vicinity of the first piston; material on the free boundary is under compression for essentially zero time. (The time required for a backscattered wave to retraverse the compressed system sets the true upper limit on the time that any region in such a simulation can be sustained in the shocked state.) The proposed *absorbing boundary condition* described here minimizes in a practical way the effects of wave reflection from a free surface, effectively providing a near-perfect impedance match[17] between the target material and the two pistons, and thus, allows simulation of the sample in a shock-compressed state for an interval of time whose limit is determined by the stability of the numerical integration scheme.

B. Model system and details of simulation procedure

For demonstration purposes, we have chosen to study shock-induced chemistry in methane as predicted by the AIREBO potential due to Stuart *et al.*[15] AIREBO is an extension of the reactive empirical bond order potential.[18]

AIREBO was designed to optimally describe liquid-state hydrocarbon properties at ambient pressure, while perturbing as little as possible predictions for the solid-state polymorphs of pure carbon. AIREBO has been used previously in MD studies of thermal dissociation in methane, ethylene, and benzene,[19] and of shock-induced chemistry in solid acetylene,[20,21] ethylene,[20] methane,[20,21] and anthracene.[21] The MD simulations presented here were performed using a computer code developed for AIREBO by Stuart *et al.* Trajectories were integrated using the velocity Verlet algorithm, with step sizes in the interval from 0.1 to 0.25 fs depending on the temperature and pressure.

The simulation cell for the shock wave simulations consists of $82\times3\times3$ unit cells of methane phase I, a face-centered-cubic (fcc) unit cell with rotating molecules at the lattice sites.[22] Initially, all atoms were positioned on the perfect fcc lattice with no orientational disorder. Next, the system was equilibrated in the *NVT* ensemble, with periodic boundary conditions applied in the directions transverse to the direction of subsequent shock loading, and cell parameters adjusted to yield zero pressure at a given temperature; a gap of 11.722 Å (two unit cell widths) was introduced between the first and second layers of unit cells along the shock direction. Atoms in the first and last layers of unit cells along the shock direction, which comprise piston-1 and piston-2, respectively, were held fixed during this equilibration period, which was continued until the system reached steady-fluctuating values about the prescribed temperature. Shock waves were generated by driving piston-1 into the target sample with constant velocity u_p. Piston-2, on the opposite end of the sample, was initially assigned zero velocity. Both pistons were perfectly rigid.

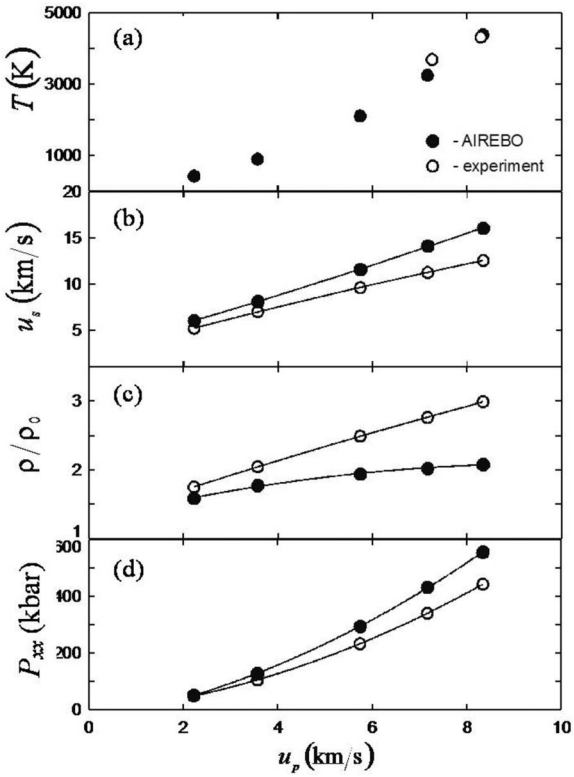

FIG. 3. Shock strength dependence of (a) temperature, (b) shock speed, (c) compression ratio, and (d) shock pressure in liquid methane. The initial temperature and density are 111 K and 0.42 g/cm^3, respectively. Solid symbols, simulation predictions, open symbols, experiment. Data for pressure, compression ratio, and shock velocity are from Nellis *et al.* (Ref. 23); temperature measurement is from Radousky *et al.* (Ref. 24).

III. RESULTS AND DISCUSSION

A. Comparison of adaptive intermolecular reactive empirical bond order predictions to experimental results

We provide details of the validation of the absorbing boundary condition in Sec. III B. In this section, we present a comparison between AIREBO predictions obtained using the absorbing boundary condition and experimental shock wave data[23,24] for liquid methane at initial temperature 111 K and density 0.42 g/cm^3; the results are summarized in Fig. 3. The shock temperature predicted for AIREBO is in good agreement with experiment [Fig. 3(a)]. Figure 3(b) indicates that the AIREBO potential overestimates the shock speed by ~25% for u_p=8.3 km/s, whereas the compression ratio ρ/ρ_0 in Fig. 3(c) is underestimated by ~30% at that same piston velocity. Finally, the component of stress along the shock direction P_{xx} (hereafter referred to as shock pressure) behind the shock front is overestimated by about 25% at the highest piston velocity considered [see Fig. 3(d)]; this discrepancy tends to zero with decreasing piston velocity. Since temperature is the dominant thermodynamic variable for chemistry, the agreement in Fig. 3(a) suggests that shock-induced reactions predicted for methane by AIREBO may be reasonable, and are certainly sufficient for the present goal of methods development.

B. Validation of the absorbing boundary condition

Figure 4 contains plots of density, material velocity, internal energy, and temperature profiles for subvolumes of the simulation cell along the shock direction, at times before and after the second piston begins to move. The results, eight snapshots in time, are for a u_p=3.0 km/s shock in crystalline methane equilibrated at 50 K and zero pressure. Traces for successive times are shifted vertically along the ordinate as an aid to the eye. In this case, the shock wave reaches the second piston at $t=\sim5.57$ ps (bold trace in Fig. 4), at which time piston-2 is assigned a velocity u_p. Whereas this would be the maximum time (or, at best, half the maximum time) accessible by other NEMD shock methods, with the exception of that of Zhao *et al.*,[14] in the present case, the simulation was continued for an additional 30 ps. One can see from Fig. 4 that spatial distributions of the density, local mass velocity, and temperature are essentially constant over the entire time interval after the second piston starts to move. The profiles of internal energy—which are the basis for determining when the shock wave traverses the sample boundary into the second piston—have a negative slope across the simulation cell during shock wave passage. In this case, the slope is approximately preserved immediately after the second piston begins to move, but disappears within 5 ps. There is no evidence in any of the results shown in Fig. 4 for

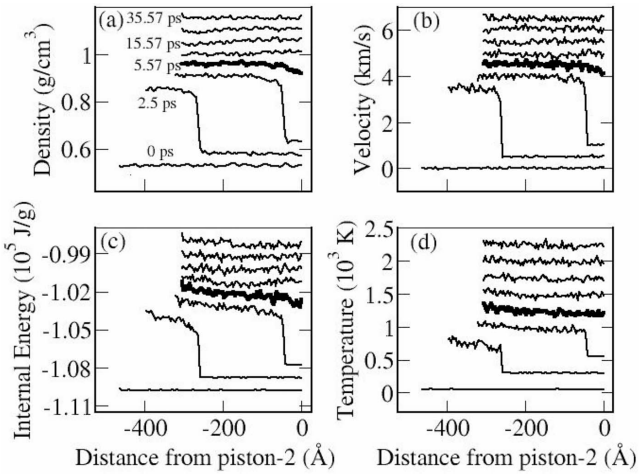

FIG. 4. Spatial profiles of (a) density, (b) local velocity, (c) internal energy, and (d) temperature along the shock direction, for eight time snapshots before and after the absorbing boundary condition is applied to shocked solid methane. The piston velocity is 3 km/s and the initial temperature is 50 K. The absorbing boundary condition is applied at $t=5.57$ ps (bold trace in the figures). Traces for successive snapshots are shifted vertically for clarity.

significant reflections or buildup of energy at either piston-sample boundary.

In Fig. 5, we compare results obtained using the absorbing boundary condition to those obtained using a standard[1] NEMD shock simulation. The only difference between the simulations is that the sample length in the latter case is twice as long as in the former. Both sets of results correspond to $t=10.0$ ps, which is just prior to the point of maximum compression in the longer cell (black lines) and 4.43 ps

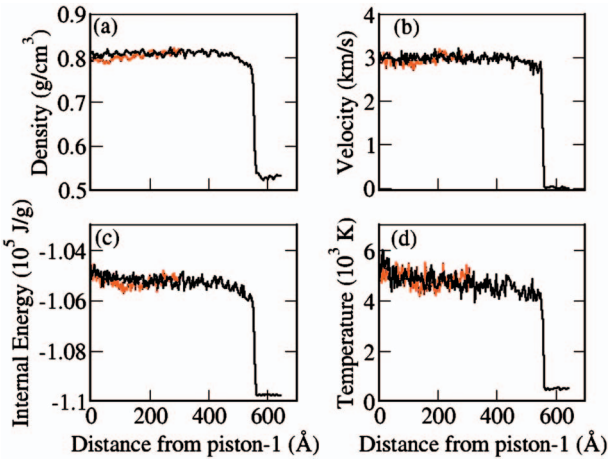

FIG. 5. (Color) Spatial profiles of (a) density, (b) local velocity, (c) internal energy, and (d) temperature along the shock direction at time $t=10.0$ ps for two simulations of shocked methane crystal differing only in the initial sample length. Red lines correspond to the simulation discussed in connection with Fig. 4, for which the absorbing boundary condition was applied at $t=5.57$ ps; black lines correspond to a system twice as long in the shock direction, which has not reached maximum compression by the end of the simulation. The piston velocity is 3 km/s and the initial temperature is 50 K.

after piston-2 was applied in the smaller one (red lines). Thus, this comparison provides a direct test of the absorbing boundary condition approach. While there are observable deviations for density, local mass velocity, internal energy, and temperature in the regions of Fig. 5 for which computational domains overlap, they are small and insignificant considering their magnitude in light of the pre- and postshock states of the material.

One can estimate the length of system that would be required, using a standard NEMD simulation, to obtain results comparable to those shown in Fig. 4; that is, one in which a shocked state is sustained for 30 ps. For $u_p=3.0$ km/s, ~5.5 ps is required for the shock wave to traverse the ~47.5 nm sample length, which means that a simulation cell of length ~260 nm would be needed. Simulation of a system of this size using a complicated reactive potential-energy function is impractical with current computing capabilities even for a single shock-passage time, let alone for the long times required to approach chemical equilibrium (e.g., ~150 ps in the following example, and in many cases, much longer).

C. Chemically reactive waves in methane

Analyses of shock-induced chemical transformations were performed for the cases $u_p=8.3$ and 11.0 km/s for shocked liquid and solid methane, respectively, based on an *ad hoc* geometric definition of molecular connectivity. Specifically, it was assumed that carbon atoms are chemically bonded when their separation is within the cutoff distance for the intramolecular interactions in the AIREBO potential function.[15] Thus, a molecule is defined as the set of carbon atoms for which any two members of that set can be linked to all other members through an unbroken sequence of bonds. Within this framework, we define isolated carbon monomers, dimers, trimers, etc., as having molecular sizes 1, 2, 3, etc.

Examination of molecular sizes after shock wave propagation through liquid methane for $u_p=8.3$ km/s indicates that initial ethane production occurs with a latency of ~3 ps after shock wave passage. (Recall that the shock wave traversal time for the entire sample is only about 5.5 ps.) The study of several specific reaction events reveals a propensity for ethane formation to occur by two unimolecular dissociation events: $2CH_4 \rightarrow 2CH_3+2H$ followed by recombination to yield $C_2H_6+H_2$. This result is in agreement with tight-binding MD simulations[25] and experimental measurements of temperature[24] and conductivity[26] behind the shock front. Given that molecular dissociation is thermally activated, it is not surprising that moderate differences between the calculated and experimental pressures have comparatively small effects on the predicted reaction thresholds and chemistry.

The decomposition threshold for solid methane using AIREBO is $u_p=9$ km/s, for which the shock temperature is ~4600 K. This temperature is close to the value observed in liquid methane shock propagation, 4400 K [see Fig. 4(a)]. Elert *et al.*[20] carried out MD simulations of shock wave propagation in solid methane and reported a somewhat higher value, 10 km/s, for the decomposition threshold ve-

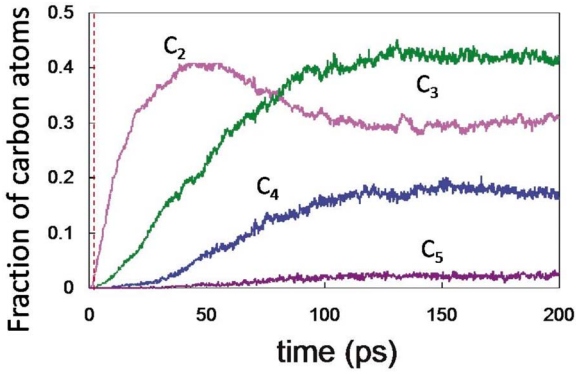

FIG. 6. (Color online) Time dependence of molecular carbon cluster size in solid methane shocked with a piston velocity u_p =11 km/s. The initial temperature and density were 50 K and 0.53 g/cm^3, respectively. Curves C_2, C_3, C_4, and C_5 correspond nominally to ethane, propane, isomers of butane, and isomers of pentane, respectively. The vertical dashed line at t=2.2 ps indicates the time at which the second piston began to move.

locity. This discrepancy is likely caused by the different approach used for shock wave initiation in those simulations: a finite flyer plate of several unit cells thickness was used, which resulted in rarefaction waves entering the compressed region and, thus, decreasing the time available for reaction to occur in the fully compressed state, whereas the initiating piston used here emulates a macroscopic striker.

In Fig. 6, we show the time evolution of carbon molecular sizes for solid methane shocked at u_p=11 km/s. The shock wave traversal time is only about 2.2 ps (denoted by the vertical line in the figure). Though most of the carbon atoms in the system are members of three-atom molecules (i.e., propanelike chains, C_3), about 20% are involved in clusters containing four or more atoms and about 25% of all carbon atoms belong to clusters consisting of more than 50 carbon atoms. Diamond anvil cell experiments in which infrared absorption, Raman spectroscopy, and x-ray diffraction were measured indicate that diamond and hydrogen, as well as hydrocarbon polymer chains, are formed from methane upon static compression in the interval of 10–50 GPa and laser heating to 2000–3000 K.[27] It is likely that the system studied here at t=200 ps represents an early stage on the transformation path toward diamond+H_2, an overall process characterized by diffusion-limited rates with time constants and spatial scales that exceed those of the present simulation.

IV. SUMMARY AND CONCLUSIONS

We have developed a practical approach for nonequilibrium molecular dynamics simulations of shock waves that allows the study of shocked states for time scales far larger than the shock wave traversal time of the MD simulation cell. A shock wave is generated by driving a rigid piston into a sample at constant piston velocity. A second rigid piston is located at the opposite end of the simulation cell, contiguous to and equilibrated with the material. When the shock wave reaches the end of the simulation cell, the second piston begins to move at the same velocity as the first and, thus, provides an "impedance match" for the shock wave across the sample-piston interface. With both pistons moving at the same velocity, the Hugoniot state of the shocked material is sustained, while the sample continues to evolve. This allows a significantly longer simulation without significant interference from reflected waves that arise at interfaces. The principal distinction between the present method and the one due to Zhao *et al.*[14] is the extent to which the present one should be extendable to treat split wave structures, for instance, an elastic precursor followed by a plastic wave, or to accommodate inhomogeneous wave profiles that might require finite piston acceleration profiles, which themselves might vary across the surface of the piston (e.g., a shock wave propagating along the longitudinal axis of a hexagonal-cylindrical microphase segregated copolymer morphology).

We applied this absorbing boundary condition approach to shock waves in methane, modeled using the AIREBO force field.[15] We demonstrated that the method does not introduce significant fluctuations in density or local velocity across the simulation cell or at the piston-sample interfaces, and that the internal energy (which is the criterion upon which the time to start the second piston moving is based) is equilibrated on a several picosecond time scale. We illustrated the practical usefulness of the method by simulating shock-induced chemistry in methane on a 200 ps time scale, for a simulation cell with a shock wave traversal time of only 2.2 ps. While the simple implementation of the absorbing boundary condition described here involves infinite acceleration of the second piston, adaptations to provide more sophisticated "soft catches" should be straightforward. We expect this general approach to be useful for simulations of shock-induced dynamics including chemistry in various materials, with numerical integration stability and, of course, the validity of the classical approximation being the limiting factors.

ACKNOWLEDGMENTS

We are grateful to Don Brenner, Steve Stuart, Marc Cawkwell, Ed Kober, Sam Shaw, Ali Siavosh-Haghighi, and Jenel Vatamanu for several fruitful discussions. We are especially grateful to Steve Stuart for providing a copy of his code along with personal instructions for using it. L.Z. is grateful for Wei Yang's support. This work was supported by a DOD MURI grant managed by the Army Research Office. T.D.S. was supported by the U.S. Department of Energy under Contract No. DE-AC52-06NA25396 with Los Alamos National Security, LLC.

*Present address: Institute of Theoretical and Applied Mechanics, Institutskaja Strasse 4/1, Novosibirsk 630090, Russia.
†Present address: School of Computational Science, Florida State University, Tallahassee, FL 32306.
‡thompsondon@missouri.edu
§sewell@lanl.gov

[1] B. L. Holian, Shock Waves **5**, 149 (1995); **13**, 489 (2004).
[2] E. M. Bringa, K. Rosolankova, R. E. Rudd, B. A. Remington, J. S. Wark, M. Duchaineau, D. H. Kalantar, J. Hawreliak, and J. Belak, Nat. Mater. **5**, 805 (2006).
[3] K. Kadau, T. C. Germann, P. S. Lomdahl, and B. L. Holian, Science **296**, 1681 (2002).
[4] B. L. Holian, T. C. Germann, J.-B. Maillet, and C. T. White, Phys. Rev. Lett. **89**, 285501 (2002).
[5] A. J. Heim, N. Gronbech-Jensen, T. C. Germann, E. M. Kober, B. L. Holian, and P. S. Lomdahl, Phys. Rev. E **76**, 026318 (2007).
[6] T. C. Germann, B. L. Holian, K. Kadau, and P. S. Lomdahl, *Lecture Series in Computer and Computational Sciences* (VSP BV, AH Zeist, Netherlands, 2005), Vol. 4A-4B, p. 1138.
[7] A. Strachan, A. C. T. van Duin, D. Chakraborty, S. Dasgupta, and W. A. Goddard III, Phys. Rev. Lett. **91**, 098301 (2003).
[8] J.-B. Maillet, M. Mareschal, L. Soulard, R. Ravelo, P. S. Lomdahl, T. C. Germann, and B. L. Holian, Phys. Rev. E **63**, 016121 (2000).
[9] E. J. Reed, L. E. Fried, and J. D. Joannopoulos, Phys. Rev. Lett. **90**, 235503 (2003).
[10] E. J. Reed, L. E. Fried, M. R. Manaa, and J. D. Joannopoulos, in *Chemistry at Extreme Conditions*, edited by M. R. Manaa (Elsevier, New York, 2005), pp. 297–328.
[11] R. Ravelo, B. L. Holian, T. C. Germann, and P. S. Lomdahl, Phys. Rev. B **70**, 014103 (2004).
[12] F. Barmes, L. Soulard, and M. Mareschal, Phys. Rev. B **73**, 224108 (2006).
[13] V. V. Zhakhovskiĭ, S. V. Zybin, K. Nishihara, and S. I. Anisimov, Phys. Rev. Lett. **83**, 1175 (1999).
[14] S. Zhao, T. C. Germann, and A. Strachan, J. Chem. Phys. **125**, 164707 (2006).
[15] S. J. Stuart, A. B. Tutein, and J. A. Harrison, J. Chem. Phys. **112**, 6472 (2000).
[16] The absorbing boundary condition approach presented in this paper should not be confused with other approaches in the computational physics literature, wherein artificial zones are introduced at the boundaries of a computational domain to damp out waves at the simulation boundary; for example, the use of negative imaginary potentials at the edges of the grid in simulations of quantum wave packets.
[17] Mathematically, acoustic impedance is defined as $k=\rho c$, where ρ is density and c is sound speed. The difference between acoustic impedances at a material interface determines the amount of energy transmitted and reflected at that interface. Our use of "near perfect impedance match" in the present context refers to the absence of significant reflected waves due to the presence of the second piston and its infinite acceleration from zero to u_p.
[18] D. W. Brenner, Phys. Rev. B **42**, 9458 (1990).
[19] J. A. Viecelli and J. N. Glosli, J. Chem. Phys. **117**, 11352 (2002).
[20] M. L. Elert, S. V. Zybin, and C. T. White, J. Chem. Phys. **118**, 9795 (2003).
[21] M. L. Elert, S. V. Zybin, and C. T. White, in *Chemistry at Extreme Conditions*, edited by M. R. Manaa (Elsevier, New York, 2005), pp. 351–368.
[22] R. M. Hazen, H. K. Mao, L. W. Finger, and P. M. Bell, Appl. Phys. Lett. **37**, 288 (1980).
[23] W. J. Nellis, F. H. Ree, M. van Thiel, and A. C. Mitchell, J. Chem. Phys. **75**, 3055 (1981).
[24] H. B. Radousky, A. C. Mitchell, and W. J. Nellis, J. Chem. Phys. **93**, 8235 (1990).
[25] J. D. Kress, S. R. Bickham, L. A. Collins, B. L. Holian, and S. Goedecker, Phys. Rev. Lett. **83**, 3896 (1999).
[26] W. J. Nellis, D. C. Hamilton, and A. C. Mitchell, J. Chem. Phys. **115**, 1015 (2001).
[27] L. R. Benedetti, J. H. Nguyen, W. A. Caldwell, H. Liu, M. Kruger, and R. Jeanloz, Science **286**, 100 (1999).